



A comparative study of novel chalcone derivative by X-ray and quantum chemical calculations (Ab-initio and DFT): Experimental and theoretical approach

Urmila H. Patel, Sahaj A. Gandhi, Vijay M. Barot & Mitesh C. Patel

To cite this article: Urmila H. Patel, Sahaj A. Gandhi, Vijay M. Barot & Mitesh C. Patel (2016) A comparative study of novel chalcone derivative by X-ray and quantum chemical calculations (Ab-initio and DFT): Experimental and theoretical approach, *Molecular Crystals and Liquid Crystals*, 624:1, 190-204, DOI: [10.1080/15421406.2015.1011494](https://doi.org/10.1080/15421406.2015.1011494)

To link to this article: <http://dx.doi.org/10.1080/15421406.2015.1011494>



Published online: 11 Feb 2016.



Submit your article to this journal [↗](#)



Article views: 57



View related articles [↗](#)



View Crossmark data [↗](#)

A comparative study of novel chalcone derivative by X-ray and quantum chemical calculations (Ab-initio and DFT): Experimental and theoretical approach

Urmila H. Patel^a, Sahaj A. Gandhi^b, Vijay M. Barot^c, and Mitesh C. Patel^c

^aDepartment of Physics, Sardar Patel University, Vallabh Vidyanagar, Gujarat, India; ^bCenter for Interdisciplinary Studies in Science and Technology (CISST), Sardar Patel University, Vallabh Vidyanagar, Gujarat, India; ^cP. G. Center in Chemistry, Smt. S. M. Panchal Science College, Talod, Gujarat, India

ABSTRACT



A novel bio-organic molecule, 3-(3-chloro-4-methoxy-phenyl)-1-(4,5-dimethoxy-2-methyl phenyl) prop-2-en-1-one (I), has been synthesized and characterized by FTIR, ¹H, and ¹³C NMR. To understand the role of solvents, UV-vis absorption, and fluorescence study has been carried out using different solvents. The single-crystal X-ray diffraction technique has been studied to confirm the three dimensional structure of the compound and the hydrogen bond interactions involved in the stability of the structure. The ab-initio and density functional theory (DFT) are used to optimize the molecular structure. The calculated results show that the predicted geometry can well reproduce structural parameters. In addition, frontier molecular orbitals and Mullikan charge distributions are carried out by using RHF and B3LYP methods. The synthesized compound has been screened for its antimicrobial and antifungal activities against different panel of organisms.

KEYWORDS

Chalcones; UV-visible & fluorescence; Single crystal X-ray diffractions; *Ab-initio* & DFT calculations; Antimicrobial & Antifungal activities

1. Introduction

Chalcones, belonging to flavonoid family, prop-2-en-ones, are obtained from both synthesis and natural sources. Chalcones consist of two aromatic rings connected by α , β -unsaturated carbonyl group. They have wide spectrum of biological activities such as anti-cancer [1], anti-malarial [2], anti-inflamentry [3], anti-HIV [4], anti-oxidant [5], anti-bacterial [6], anti-fungal [7], anti-viral [8] anticonvulsant [9], and anti-hyperglycemic [10]. Beyond these very important application in medical and pharmacy, chalcones have interesting UV and florescent optical properties [11]. Nowadays, quantum chemical calculations have been established to be an important tool to study the relationship between structural properties of organic molecules and for the interpretation of experimental data arising from industrial interest and applications [12]. The ab-initio and density functional theory (DFT) have been applied for investigation of the optimized molecular structure and few interesting significant spectroscopy properties. As a part of our ongoing research on synthesis of novel bio-organic molecules and their theoretical quantum chemical computational studies [13], here we wish to report the synthesis

CONTACT Sahaj A. Gandhi  sahajg7@gmail.com  Center for Interdisciplinary Studies in Science and Technology (CISST), Sardar Patel University, Vallabh Vidyanagar 388120, Gujarat, India.

Color versions of one or more of the figures in the article can be found online at www.tandfonline.com/gmcl.

© 2016 Taylor & Francis Group, LLC

of novel chalcone derivative (methoxy, ethoxy, and halogen (Cl) substituted) with the characterizations of IR, ^1H and ^{13}C NMR. We also included X-ray crystallographic investigations of the compound to find out the exact position of the different substituent. The optimization of the structure of the compound has been performed by RHF and B3LYP methods at 6–311G basis set level using Gaussian-09 software package. To understand pharmacological applications on structural basis, we evaluated antimicrobial and antifungal activities of the synthesized product against different panel of organisms.

2. Experimental section

2.1. Materials and methods

All chemicals (AR grade) were commercially available and used without further purification unless otherwise stated. Melting points were determined on an electro thermal melting point apparatus. Completion of reaction and purity of all compounds were checked on aluminum coated TLC plates 60 F245 (E. Merck) using *n*-hexane: ethyl acetate (7.5:2.5, v/v) as mobile phase and visualized under ultraviolet (UV) light, or iodine vapor. Elemental analysis (% C, H, N) was carried out by a Perkin-Elmer 2400 CHN analyzer. IR spectra recorded on a Perkin-Elmer FT-IR spectrophotometer in KBr. ^1H NMR and ^{13}C NMR spectra were recorded on a Varian Gemini 300 MHz and Varian Mercury-400 (100 MHz) in DMSO- d_6 as a solvent and tetramethylsilane (TMS) as an internal standard respectively. Mass spectrum was scanned on a Shimadzu LCMS 2010 spectrophotometer. UV-visible absorption measurements of the synthesized compound over a wavelength ranges 200–800 nm were recorded on a Shimadzu, Japan (UV-160) spectrometer. The luminescence spectra were measured using a Perkin Elmer LS 55 Fluorescence Spectrometer.

2.2. Synthesis

A mixture of 1-(2-methyl-4, 5-dimethoxyphenyl) ethanone (0.01 mole) and substituted benzaldehyde (0.01 mole) in ethanol (30 ml) was added a solution of potassium hydroxide (40 ml, 40%) with constant shaking of the reaction flask. The reaction mixture was stirred for a 24 hours on a magnetic stirrer and poured in to crushed ice and acidified with diluted HCl (2N). The solid mass product was filtered and separated, washed with water, dried in a vacuum and crystallized from methanol to give light yellow needles. Completion of reaction were checked on aluminum coated TLC plates 60 F245 (E. Merck) using *n*-hexane: ethyl acetate (7.5:2.5, v/v).

2.3. Characterization of compound

3-(3-chloro-4-methoxy-phenyl)-1-(4,5-dimethoxy-2-methyl phenyl)prop-2-en-1-one (I)

Yield: 65%; m.p.130–136°C; IR (cm^{-1}): 2931 (C–H str. (asym) alkyl), 2862 (C–H str. (sym) alkyl), 1455 (C–H def (asym) alkyl), 1377 (C–H def (sym) alkyl), 3067 (C–H str.arom.), 1498. (C=C str. arom.), 1263 (C–O–C (sym) ether), 1030 (C–O–C (asym) ether), 1705 (C=O str., chalcone), 3361 (OH, phenol), 900 (CH=CH def.chalcone), 3067 (CH=CH str. chalcone), 1620 (C=C str. chalcone), 682 (C–Clstr.). ^1H NMR (CDCl_3) δ ppm: 2.44 (s, 3H), 3.89 (s, 3H, OCH_3), 3.91 (s, 3H, OCH_3), 3.93 (s, 3H, OCH_3), 6.76(s,1H),6.94(d,1H, $J=8.5\text{Hz}$),7.06(m,1H+1H chalcone, merged),7.419–7.459(m,1H+1H chalcone, merged),

7.62(d, 1H, $J=2.0\text{Hz}$). ^{13}C NMR (CDCl_3) δppm : 55.88(C-1), 56.17(C-2), 56.27(C-3), 20.55(C-4), 193.71(C-5), 127.54(C-6), 146.40 (C-7), 139.06(C-8), 136.30(C-9), 151.21(C-10), 146.40(C-11), 132.06(C-12), 114.25(C-13), 112.41(C-14), 128.38(C-15), 129.20(C-16), 129.97(C-17), 131.77(C-18), 129.77(C-19).

LCMS m/z : 347 ($M+1$). Anal. calc. for $\text{C}_{19}\text{H}_{19}\text{ClO}_4$ found (%): C, 65.79; H, 5.54; X : 10.23.

2.4. X-ray crystallography

The three dimensional X-ray intensity data of the crystal was collected on a Bruker KAPPA APEX-II CCD-4 diffractometer. The cell refinement and data reductions has been obtained using Bruker SAINT programme. The structures has been solved by direct methods and refined by full matrix least squares technique based on F^2 using SHELXS-97 and SHELXL-97 built in WinGX programme package. [14] Non-hydrogen atoms have been refined anisotropically. The H atoms positions are geometrically fixed. These H atoms have been constrained to ride on their parent atoms with $\text{Uiso}(\text{H}) = 1.2\text{Ueq}(\text{C})$ for the phenyl H atoms and $\text{Uiso}(\text{H}) = 1.5\text{Ueq}(\text{C})$ for the methyl H atoms. PLATON software was used for molecular graphics [15].

2.5. Antimicrobial and antifungal activities

The synthesized compound has been screened for their antibacterial activity against Gram-positive bacteria (*Staphylococcus aureus* (MTCC-96), *Streptococcus pyogenes* (MTCC-442)) and Gram negative *E. coli* (MTCC-443), *Pseudomonas aeruginosa* (MTCC-1688)). Antibacterial activity was measured as per National Committee for Clinical Laboratory Standards (NCCLS) protocol by Mueller–Hinton Broth [16]. The highest dilution (lowest concentration) preventing appearance of turbidity has been taken as MIC i.e., the amount of growth from the control tube before incubation (which represents the original inoculums) has compared. For bacterial growth, in the present protocol, we have used Muller Hinton broth at 37°C in aerobic condition for 24–48 hours. Also, the compound has been tested for antifungal activity against *Candida albicans*. For fungal growth, in the present protocol, we have used Sabourauds dextrose broth at 28°C in aerobic condition for 48 hours.

3. Results and discussion

3.1. Synthesis

A procedure based on a Claisen–Schmidt condensation has been developed for the synthesis of chalcone derivative, illustrated in Fig. 1. Substituted aldehyde and ketones have been condensed to form chalcones using potassium hydroxide as a catalyst in methanol at room

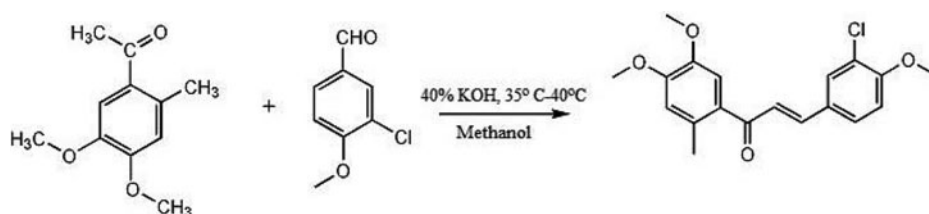


Figure 1. Synthesis of chalcone derivative, reaction Conditions: 40% potassium hydroxide (KOH) as a catalyst in methanol at 35°C – 40°C .

temperature. The product has been formed immediately after addition of the potassium hydroxide to the stirred mixture of aldehyde and ketone. A minimal amount of methanol solvent has been used for the formation of product in the solid form. The α , β -unsaturated ketones have been the trans-alkene (E form) as judged by ^1H NMR spectroscopy.

The Infrared spectrum has been recorded on the KBr disc in order to avoid the shoulder formation on carbonyl doublets. The s-cis conformers exhibited higher frequencies than the s-trans conformers due to the bulky group causes greater strain. The correlation conjugation between the $\text{C}=\text{O}$ and the $-\text{CH}=\text{CH}-$ parts has been failed due to non co planarity arising out of non bonded repulsion between both the styryl parts in the systems and the cross conjugation of phenyl ring. Due to the extended conjugation, the phenyl ring reduces the correlation on carbonyl frequencies. The observation that H_α protons appeared at higher field than that of H_β protons made the subject very interesting, this may possibly due to the polarization of $\text{C}=\text{C}$ double bond in the system being predominantly caused by the carbonyl group so as to make electron density at a position greater than that of β position.

3.2. UV- visible and florescent spectroscopic study

In order to evaluate solvent effects on the absorption spectra, fundamental UV/Vis characterization has been carried out. The electronic spectra of compound has recorded in ethanol, chloroform and DMSO (10^{-3} M) solvents and showed charge-transfer absorption band in the UV-region. Most of the absorption spectroscopy of the compound has been based on the transitions of n or π electrons to the π^* excited states which take place in the range of 200–400 nm. The results exhibited an intense absorption in the UV-region and the positions of maximum peak depend on the different solvents. The solvent also plays an important role in the absorption study. Figure 2 shows the absorption spectra of the compounds in ethanol, chloroform and DMSO solvents. Figure 2 shows the absorption spectra have displayed two maxima absorption wavelength peaks (250 to 270 nm and 300 to 320 nm). The nature of the absorption curve for DMSO and CHCl_3 is almost same, but slightly different in Ethanol. To compile all the absorption spectra of different solvents, it can conclude that the absorption spectra for the compound in DMSO solution was red shifted as compared to other solvents viz, chloroform and ethanol, indicating relatively strong guest–host interaction between the molecules and the DMSO environment. It is due to different interactions between the solute and solvent.

We also measured the emission characteristics of compound in DMSO illustrated in Fig. 3 and observed the wavelength maxima λ_{max} at 515nm.

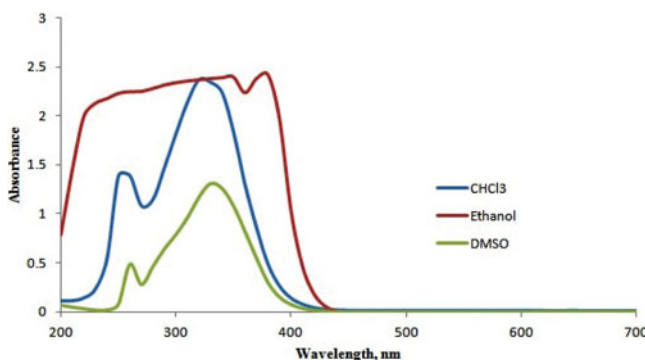


Figure 2. UV-Vis spectra of compound in different solvents Ethanol, Chloroform, and DMSO.

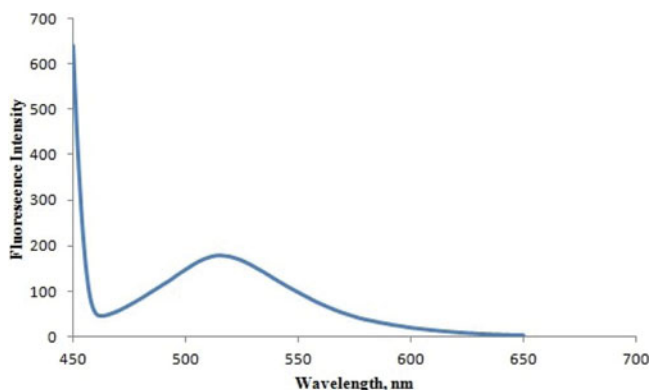


Figure 3. Fluorescence emission spectra of compound in DMSO ($\lambda_{em} = 515$ nm).

3.3. X-ray diffraction study

The crystal and molecular structures of the compound has been investigated by X-ray crystallographic technique. The slow evaporation method has been used to grow the single crystals. Yellow colored pentagonal shaped single crystals of compound have been grown using ethanol solvent. Density of crystal has 1.356 Mg/m^3 measured by flotation method using potassium iodide (KI) solution. The title compound, $\text{C}_{19}\text{H}_{19}\text{ClO}_4$ crystallized in triclinic system of space group P-1. An 'ORTEP' view of the compound with atomic numbering scheme (thermal ellipsoids drawn at 50% probability level) has shown in Fig. 4. The crystallographic data and details of the data collection and structure refinements are listed in Table 1. The selected bond lengths, bond angles, and torsional angles of the compound are tabulated in Table 2.

In the molecule, 3-(3-chloro-4-methoxy-phenyl)-1-(4,5-dimethoxy-2-methylphenyl) prop-2-en-1-one, Chlorine and methoxy group were attached on 3rd and 4th position of the phenyl ring respectively. In the crystal structure, the bond lengths of C2-Cl7 , C10=C11 , and C12=O13 has $1.7337(14)$, $1.3282(2)$, and $1.2235(19) \text{ \AA}$, respectively. The dihedral angles between both the phenyl rings (C1-C6) and (C14-C19) has $48.82(7)^\circ$. Two intra molecular

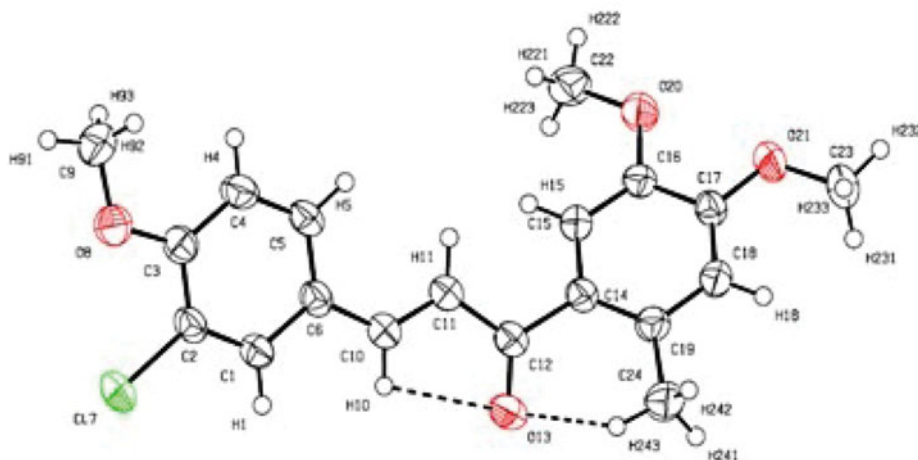


Figure 4. ORTEP diagram of the compound (I), showing 50% probability displacement ellipsoids.

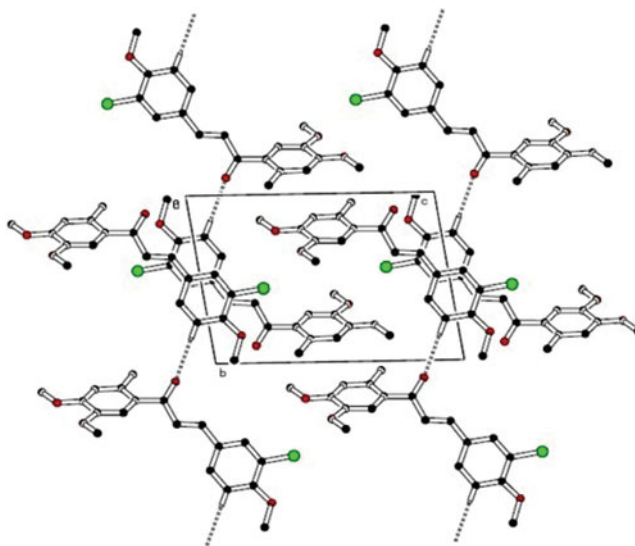


Figure 5. Stereo view of part of the crystal structure of title compound, showing the formation of a C–H ...O hydrogen bond interactions.

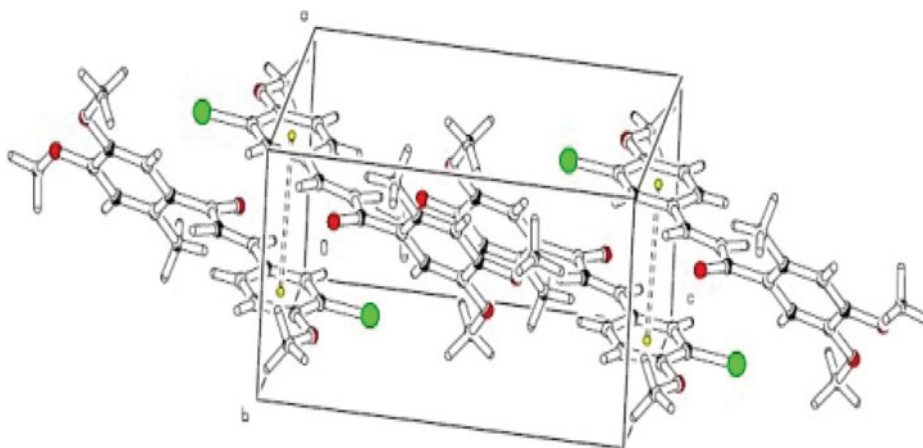


Figure 6. Molecular packing diagram shows π – π interactions.

interactions C10–H10...O13 and C24–C243...O13 has been observed in the title structure (Fig. 3) lead to the formation of pseudo-five S(5) and pseudo-six S(6) graph set motif hydrogen-bond pattern [17]. Molecular conformation about C6–C10, C10–C11, C11–C12, and C12–C14 bonds described by the torsional angles C5–C6–C10–C11, C6–C10–C11–C12, C10–C11–C12–C14, and C11–C12–C14–C16 were $-2.8(3)^\circ$, $176.08(14)^\circ$, $175.66(14)^\circ$, and $136.67(15)^\circ$, respectively. The hydrogen bond geometry of the compound is presented in Table 3. The stability of the title compound has been due to the network of strong C–H ...O hydrogen bond interactions. In the crystal packing, carbon atom of the chloro phenyl ring C4 via H4 act as a potential donor to prop-2-en-1-one group of oxygen O13; C4–H4 ...O13 interactions at $(x, -1+y, 1-z)$ generated a chain along bc plane near corner of the unit cell as shown in Fig. 5. In the crystal structure, face to face π – π stacked interactions (Fig. 6) are observed between the two centroids of chloro phenyl ring (C1–C6) Cg(1) with cholro

Table 1. Crystal data and structure refinement parameters of the title compounds.

Empirical formula	C ₁₉ H ₁₉ Cl O ₄
Formula weight	346.79
Temperature /K	293(2)
Wavelength /Å	MoK α (0.71073)
Crystal system	Triclinic
Space group	P-1
Crystal size /mm	0.41 \times 0.40 \times 0.16
a/Å	7.0992(2)
b/Å	9.3464(3)
c/Å	13.2331(4)
α°	79.954(2)
β°	82.4490(10)
γ°	80.6030(10)
Cell Volume /Å ³	848.18(4)
Z	2
Calculated density Mg/m ³	1.356
Absorption coefficient mm ⁻¹	0.245
F(000)	364
θ range for data collection ($^\circ$)	1.57 to 27.57
Index ranges	$-9 \leq h \leq 9$; $-12 \leq k \leq 12$; $-17 \leq l \leq 17$
Reflections collected/unique [R(int)]	15634/ 4383 [0.0311]
Completeness to θ max (%)	0.991
Absorption correction	T _{min} = 0.8978, T _{max} = 0.9413
Refinement method	Full Matrix Least Square of $ F ^2$
Data/restraints/parameters	4383/0/ 219
Goodness-of-fit on F ²	1.041
Final R indices	R ₁ = 0.0431, wR ₂ = 0.1289
R indices (all data)	R ₁ = 0.0480, wR ₂ = 0.1363
Largest diff. peak and hole /e Å ⁻³	0.326 and -0.345

phenyl ring of Cg(1) $1-x$, $1-y$, $2-z$. The Cg–Cg separation distance of 3.8882(9) Å ($\alpha = 0^\circ$ & $\beta = 25.24^\circ$). The C–H... π interaction of type-III, involves methoxy phenyl ring carbon C22 via H221 to the centroid of the methyl phenyl ring Cg(2) of the symmetry related ($1-x$, $1-y$, $1-z$) phenyl ring (C14–C19) where C22–H221...Cg(2) = 3.692 Å and angle 137° (Table 3).

3.4. Computational details

In order to study the molecular properties of the compound, quantum chemical calculations have been performed at different level of theory. The Ab-initio and DFT calculations were carried out for the purpose of optimization geometries of the compound 2 within the framework of Hartree Fock [18] and the density functional theory with Becke's three-parameter hybrid exchange functional with Lee–Yang–Parr correlation functional (B3LYP) employing 6-311g basis set [19]. All quantum chemical calculations were calculated using computer software Gaussian-09 [20] and Gauss–View molecular visualization program [21].

3.4.1. Optimized geometry

The ab-initio and Density Functional Theory (DFT) with Gaussian-09 program package employing B3LYP (Becke three parameter Lee–Yang–Parr) method with 6-311G* basis set have been used to determine optimized bond lengths and bond angles. Comparison between the experimental (X-ray) bond lengths and bond angles with theoretical bond lengths and bond angles indicated that all optimized bond lengths and bond angles were slightly larger than the experimental values (Table 2). This was the case because the experimental data

Table 2. Bond lengths (Å), Bond angles (°), and Torsional angles (°) involving nonhydrogen atoms by X-ray data (with estimated standard deviation in parentheses) and by theoretical calculations at the RHF/6-311G and B3LYP /6-311G levels of theory.

Bond lengths (Å)	X-ray	RHF/6-311G	B3LYP/6-311G
C1—C2	1.372 (2)	1.3743	1.3823
C1—C6	1.398 (2)	1.3959	1.4119
C2—C3	1.392 (2)	1.3874	1.4020
C2—C17	1.7337 (14)	1.7950	1.8171
C3—O8	1.3529 (19)	1.3575	1.3775
C3—C4	1.397 (2)	1.3901	1.4035
C4—C5	1.385 (2)	1.3826	1.3911
C5—C6	1.393 (2)	1.3921	1.4075
C6—C10	1.457 (2)	1.4681	1.4607
O8—C9	1.411 (2)	1.4293	1.4553
C10—C11	1.328 (2)	1.3308	1.3489
C11—C12	1.480 (2)	1.4797	1.4815
C12—O13	1.2235 (19)	1.2287	1.2596
C12—C14	1.493 (2)	1.4844	1.4857
C14—C19	1.395 (2)	1.3930	1.4141
C14—C15	1.407 (2)	1.4053	1.4167
C15—C16	1.379 (2)	1.3709	1.3850
C16—O20	1.3645 (18)	1.3706	1.3896
C16—C17	1.406 (2)	1.4002	1.4130
C17—O21	1.3577 (18)	1.3614	1.3814
C17—C18	1.382 (2)	1.3776	1.3921
C18—C19	1.393 (2)	1.3992	1.4059
C19—C24	1.510 (2)	1.5105	1.5119
O20—C22	1.422 (2)	1.4236	1.4500
O21—C23	1.423 (2)	1.4266	1.4535
Bond Angles (°)	X-ray	RHF/6-311G	B3LYP/6-311G
C2—C1—C6	121.13 (13)	120.9625	120.8651
C1—C2—C3	121.19 (13)	121.2751	121.4638
C1—C2—C17	119.63 (11)	119.0084	119.2874
C3—C2—C17	119.18 (11)	119.7199	119.2488
O8—C3—C2	116.24 (14)	117.7345	118.1193
O8—C3—C4	125.59 (14)	124.0417	124.5060
C2—C3—C4	118.17 (14)	118.2236	118.1193
C3—C4—C5	120.52 (14)	120.5992	120.6245
C4—C5—C6	121.21 (14)	121.2649	121.3562
C5—C6—C1	117.76 (13)	117.6760	117.5703
C5—C6—C10	124.34 (13)	123.7697	123.8438
C1—C6—C10	117.90 (13)	118.5531	118.5858
C3—O8—C9	119.06 (14)	121.9832	119.5367
C6—C10—C11	129.08 (14)	127.6660	127.9527
C10—C11—C12	119.69 (14)	120.7271	120.6749
O13—C12—C11	121.51 (14)	121.0756	121.0411
O13—C12—C14	120.48 (14)	120.0725	119.8039
C11—C12—C14	118.00 (13)	118.8467	119.1431
C12—C14—C15	118.40 (13)	118.9267	119.4112
C12—C14—C19	121.54 (13)	121.7515	121.5672
C15—C14—C19	120.04 (13)	119.3046	119.0096
C16—C15—C14	121.17 (13)	122.0866	122.1048
O20—C16—C15	125.56 (13)	124.4881	124.9662
O20—C16—C17	115.50 (13)	116.6878	116.0884
C15—C16—C17	118.93 (13)	118.8241	118.9454
O21—C17—C16	115.45 (13)	116.6373	116.1271
O21—C17—C18	125.15 (13)	124.0250	124.6063
C18—C17—C16	119.40 (13)	119.3377	119.2665
C17—C18—C19	122.43 (13)	122.5049	122.5302
C18—C19—C14	117.91 (13)	117.9254	118.1247
C18—C19—C24	123.77 (14)	124.0302	123.7937
C14—C19—C24	118.31 (14)	118.0436	118.0805
C16—O20—C22	117.22 (13)	120.9902	118.6105
C17—O21—C23	116.90 (13)	121.5185	119.1175

Table 2. *Continued.*

Bond lengths (Å)	X-ray	RHF/6-311G	B3LYP/6-311G
Torsional Angles (°)	X-ray	RHF/6-311G*	B3LYP/6-311G*
C1-C2-C3-C4	— 0.1(2)	0.0569	0.0909
C17-C2-C3-O8	0.79(19)	179.8994	— 179.9836
C2-C3-O8-C9	— 174.97(15)	— 179.5405	— 179.9727
C4-C3-O8-C9	5.3(2)	0.292	— 0.0525
C5-C6-C10-C11	— 2.8(3)	7.8128	2.6258
C6-C10-C11-C12	176.08(14)	— 178.2218	— 178.2202
C10-C11-C12-O13	3.1(2)	10.9183	7.143
C10-C11-C12-C14	175.66(14)	— 169.8976	— 174.0959
C11-C12-C14-C15	45.30(19)	31.0787	25.5061
C11-C12-C14-C19	136.67(15)	— 150.4383	— 155.7486
C15-C16-O20-C22	175.09(14)	2.461	0.4265
C16-C17-O21-C23	177.98(14)	179.0688	179.7296
C17-C18-C19-C24	178.30(15)	— 179.0165	— 179.0239

were collected in the solid phase, whereas the computational theoretical data corresponds to the isolated molecule in gas phase [22]. The optimized geometry structure of the compound by B3LYP method is shown in Fig. 7. The highest bond length difference was 0.0613 Å and 0.0834 Å for the C2-Cl7 bond at RHF and B3LYP, respectively, where the biggest bond angle deviation 4.6185° (RHF) and 2.2175° (B3LYP) occurred in the C17-O21-C23 angle. The root mean square error (RMSE) was found to be about 0.0137 Å for RHF and 0.0251 Å for B3LYP, indicating that the bond lengths obtained by the RHF method had the strongest correlations with the experimental values. The correlation coefficient in bond lengths by RHF and B3LYP were 0.9942 and 0.9838, respectively. The root mean square errors for bond angles were 1.3444° and 0.7971° for RHF and B3LYP, respectively. The correlation coefficient in bond angles by RHF and B3LYP were 0.9125 and 0.9751, respectively. It revealed that the correlation coefficient for bond angles obtained by RHF method was smaller than that determined by B3LYP method [23]. The graphical representation of correlation between experimental versus theoretical bond lengths and bond angles were shown in Fig. 8.

3.4.2. Mulliken charge distributions

The atomic charge values have been obtained by the Mulliken population analysis. The Mulliken charge distribution of the compound has been presented in Table 4 and graphically shown in Fig. 9. It may be noted that the all oxygen atoms have negative charge and all

Table 3. Intra and intermolecular hydrogen bond interactions (distances in Å, angles in °).

A. Hydrogen bond interactions						
D-H ... A	d(D-H) Å	d(D-A) Å	d(H-A) Å		(D-H ... A)°	
C10-H10 ... O13(i)	0.93	2.780(2)	2.41		104	
C24-H243 ... O13(i)	0.96	2.932(2)	2.54		130	
C4-H4 ... O13(iv)	0.93	3.468(2)	2.54		178	
B. π - π interaction						
Cg(l)- Cg(J)	Cg(l) ... Cg(J) Å	α	β	γ	Cg(l) ... P Å	
Cg(1)- Cg(1)(ii)	3.8882(9)	0.0	25.24	25.24	3.517	
C. C-H ... π interaction						
C-H(l) ... Cg(J)	d(H-Cg) Å	d(C-Cg) Å	Y-X ... Cg°	γ°	H ... P Å	Type
C22-H221 ... Cg(2)(iii)	2.930	3.692(3)	137	17.62	2.795	III
Symmetry code						
(i) x, y, z ; (ii) $1-x, 1-y, -z$; (iii) $1-x, 1-y, 1-z$; (iv) $x, -1+y, z$.						

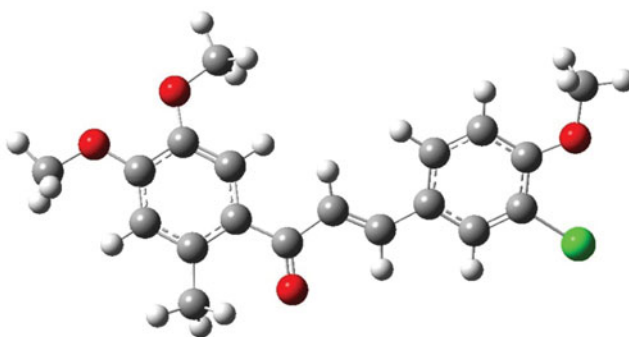


Figure 7. Optimized geometry of the title compound using B3LYP method.

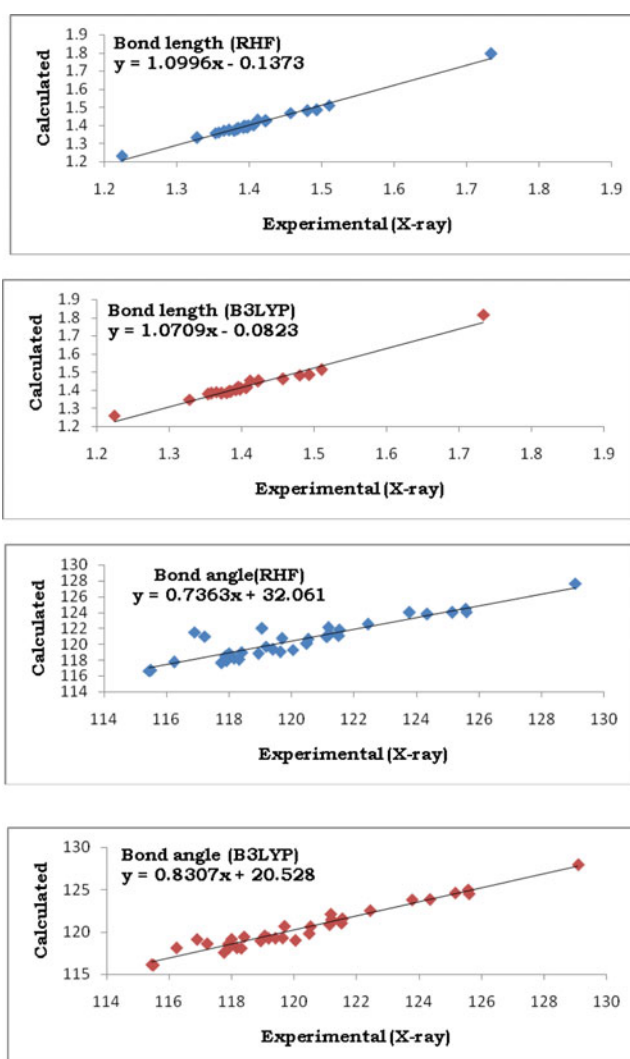


Figure 8. Correlation of calculated and experimental bond lengths and bond angles.

Table 4. Mulliken charges (e) for the title compound.

Atom	Calculated (RHF)	Calculated (B3LYP)	Atom	Calculated (RHF)	Calculated (B3LYP)
C1	−0.082651	−0.059729	C23	−0.200553	−0.295155
C2	−0.407308	−0.384964	C24	−0.525879	−0.565648
C3	0.551111	0.404517	H1	0.213666	0.194917
C4	−0.206557	−0.175591	H4	0.195565	0.177313
C5	−0.080549	−0.061799	H5	0.183613	0.162199
C6	0.013790	0.010216	H91	0.205699	0.212894
Cl7	−0.003234	0.024442	H92	0.176646	0.189947
O8	−0.675658	−0.500411	H93	0.175567	0.189053
C9	−0.199960	−0.296565	H10	0.210881	0.185272
C10	−0.118850	−0.166185	H11	0.196947	0.180244
C11	−0.268586	−0.176953	H15	0.271267	0.192463
C12	0.366307	0.167356	H18	0.198796	0.178578
O13	−0.523456	−0.395594	H221	0.196010	0.203153
C14	−0.077061	−0.022543	H222	0.170362	0.184149
C15	−0.177014	−0.149398	H223	0.160952	0.175364
C16	0.304704	0.204304	H231	0.197192	0.204645
C17	0.382111	0.253118	H232	0.171023	0.185429
C18	−0.264308	−0.201875	H233	0.172838	0.186754
C19	0.104701	0.096112	H241	0.196469	0.201525
O20	−0.664768	−0.498180	H242	0.218348	0.215193
O21	−0.662232	−0.492060	H243	0.159279	0.158460
C22	−0.201219	−0.294967			

hydrogen atoms have positive charge. The oxygen O8 atom has more negative charge than other oxygen atoms, whereas the hydrogen atom H15 had more positive charge than the other hydrogen atoms. The results suggested that the oxygen atoms were electron acceptor and charge transfer took place from H to O, which suggests that, the existence of intra and inter-molecular hydrogen bonding in the crystalline phase. The atomic charge on chlorine atom (Cl7) had -0.0032 and 0.02444 by RHF and B3LYP respectively. The chlorine atom has almost neutral, so it cannot take part in any hydrogen bond interactions. The carbon atoms C3, C12, C16, C17, and C19 had positive charge and other carbon atoms had negative charges in the molecule.

3.4.3. HOMO and LUMO analysis

Analysis of the wave function indicates that the electron absorption corresponds to the transition from the ground state to the first excited state and mainly described by electron excitation from the highest occupied molecular orbital (HOMO) to the lowest unoccupied molecular orbital (LUMO). The HOMO and its orbitals play the role of electron donors and the LUMO and its orbitals play the role of electron acceptors. HOMO and LUMO energies for the compound have been calculated by using RHF and B3LYP methods. The HOMO and LUMO plots are shown in Fig. 10. The calculated energies of HOMO and LUMO were -0.30405 and 0.04822 eV by RHF and -0.21630 and -0.08540 by B3LYP method respectively. The energy band gap of HOMO-LUMO explains the charge transfer interaction within the molecule. The values of HOMO-LUMO energies, total energy, and dipole moment of the compound are tabulated in Table 5.

3.5. Antibacterial and antifungal activities

Antimicrobials study should be inexpensive to produce using the convenient chemistry; cost of production is a critically important consideration if the resulting compounds are ever to

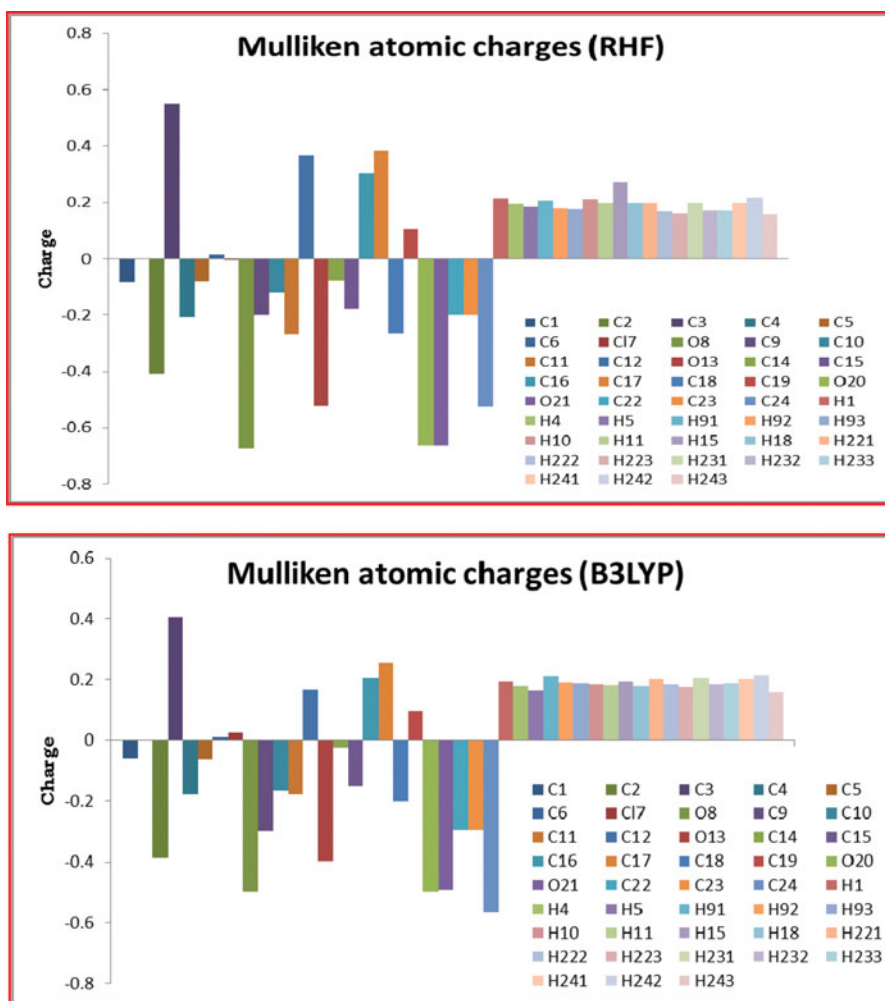


Figure 9. Graphical representations of the Mulliken charges of the title compound by RHF and B3LYP methods.

be developed into therapeutic agents for the world's developing countries. Our preliminary data and molecular efforts will be further directed and even more potent antimicrobials in the future. The observed MIC values, for bacterial and fungal strains of the compound are presented in Table 6. The MIC values reveal that the response of the drug is significant in all the panels of organisms compare to the standard drugs and exhibited good activity against fungal strain *C. albicans*.

4. Conclusion

Novel chalcone derivative has been synthesized and confirmed by chemical analysis, IR, ^1H , and ^{13}C NMR. The three dimensional structure of the compound investigated by single crystal X-ray diffraction technique. The crystal structure has been stabilized by C–H...O, C–H... π and π – π interactions. The interactions of the chalcone derivative with different solvents like ethanol, chloroform, and DMSO has been studied by UV-visible absorption spectroscopy. The predicted optimized molecular conformation was in good agreement with experimental

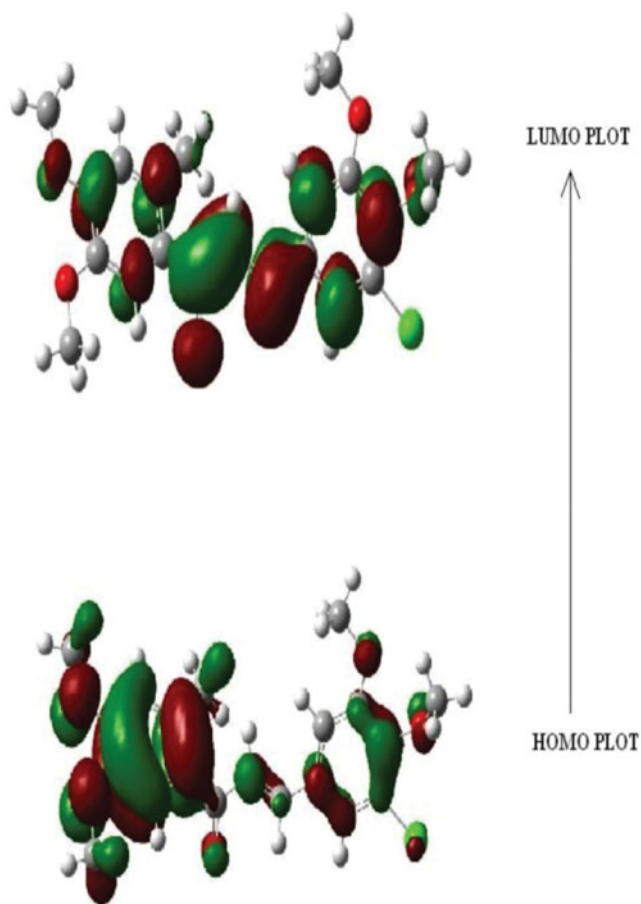


Figure 10. The highest occupied molecular orbital (HOMO) and the lowest unoccupied molecular orbital (LUMO).

Table 5. HOMO-LUMO, Total energy and Dipole moment of the compound.

Method	HOMO	LUMO	Energy Band Gap	Total Energy (Hartree)	Dipole Moment (Debye)
RHF	− 0.30405	0.04822	0.35227	− 1488.9473	5.5503
B3LYP	− 0.21630	− 0.08540	− 0.1309	− 1496.1597	5.7308

Table 6. Minimal Inhibition Concentrations of Bacterial and Fungal strains (MIC) in $\mu\text{g/ml}$.

	Bacterial and Fungal activities in Minimal Inhibition Concentrations (MIC) in $\mu\text{g/ml}$				
	<i>S. aureus</i> MTCC-96	<i>S. pyogenes</i> MTCC-442	<i>E. coli</i> MTCC-443	<i>P. aeruginosa</i> MTCC-1688	<i>C. albicans</i> MTCC-227
Present study	250	250	250	500	1000
Std. drug Gentamycin	0.05	1.0	0.25	0.5	—
Std. drug K. Nystatin	—	—	—	—	1000

results. The results from experimental and theoretical data of RMSE and correlation coefficient were in good agreement. Mulliken charge distributions analysis point out the presence of intra and intermolecular interactions involving the specific atoms. HOMO-LUMO energy band gap further supported the presence of molecular interactions, showing the charge transfer within the molecule. MIC reports revealed that the synthesized drug compound has good responses against *S. aureus*, *S. pyogenes* bacteria compared to other panel of organisms.

Supplementary Data

CCDC 984826 contains the supplementary crystallographic data for the compound. These data can be obtained free of charge via <http://www.ccdc.cam.ac.uk/conts/retrieving.html>, or from the Cambridge Crystallographic Data Centre, 12 Union Road, Cambridge CB2 1EZ, UK; fax: (b44) 1223-336-033; or e-mail: deposit@ccdc.cam.ac.uk.

Acknowledgments

We are thankful to DST, New Delhi, for providing the single-crystal X-ray diffractometer (Kappa Apex-II) under FIST facility at Department of Physics, Sardar Patel University, Vallabh Vidyanagar, Gujarat, India. We are also grateful to DSA, New Delhi for Fluorescence spectrophotometer at Department of Physics, Sardar Patel University, Vallabh Vidyanagar, Gujarat, India. Sahaj Gandhi is also thankful to UGC, New Delhi, for the financial support (RFSMS) to carry out the research work.

References

- [1] (a) Kamal, A., Ramakrishna, G., Raju, P., Viswanath, A., Janaki Ramaiah, M., *et al.* (2010). *Bioorg. Med. Chem. Lett.*, 20, 4865–4869. (b) Janel, K., Warmka Eric, L., Solberg Nicholette, A. Z., *et al.* (2012). *Biochem. Biophys. Res. Commun.* 424, 488–492. (c) Wei, H., Zhang, X., Wu, G., Yang, X., Pan, S., *et al.* (2013). *Food Chem. Toxicol.* 60, 147–152. (d) Echeverria, C., Santibañez, J. F., Donoso-Tauda, O., Escobar, C. A., *et al.* (2009). *Int. J. Mol. Sci.* 10, 221–231.
- [2] Lim, S. S., Kim, H. S., & Lee, D. U. (2007). *Bull. Korean Chem. Soc.* 28, 2495–2497. (b) Valla, B., Valla, D., Cartier, D., Le Guillou, R., Labia, R., *et al.* (2006). *Eur. J. Med. Chem.* 41, 142–146.
- [3] Okunrobo, L. O., Usifoh, C. O., & Uwaya, J. O. (2006). *Acta Poloniae Pharmaceutica - Drug Res.* 63, 195–199. (b) Chen, Yau-H., Wang, Wei-H., Wang, Yun-H., *et al.* (2013). *Molecules*, 18, 2052–2060.
- [4] Cheenpracha, S., Karalai, C., Ponglimanont, C., Subhadhirasakul, S., & Tewtrakul, S. (2006). *Bioorg. Med. Chem.* 14, 1710–1714. (b) Wu, Jiu-H., Wang, Xi-H., Yi, Yang-H., Lee, Kuo-H. (2003). *Bioorg. Med. Chem. Lett.*, 13, 1813–1815.
- [5] Tan, N. D., & Dao, T. T. (2011). *Pharmacol. Pharm.* 2, 282–288. (b) Aichaoui, H., Guenadil, F., Kapanda, CocoN., Lambert, C. R., McCurdy D. M., *et al.* (2009). *Med. Chem. Res.*, 18, 467–476.
- [6] (a) Konduru Kumar, N., Dey, S., Mohammad, S., Mohammad, O., & Naseem, A. (2013). *Eur. J. Med. Chem.* 59, 23–30. (b) Sivakumar, P. M., Cometa, S., Alderighi, M., Veluchamy, P., Doble, M., Federica, C. (2012). *Carbohydr. Polym.* 87, 353–360.
- [7] Hasan A., Rasheed, L., & Malik, A. (2007). *Asian J. Chem.* 19, 937–948.
- [8] (a) Zandi, K., Teoh, Boon-T., Sam, Sing-S., Wong, Pooi-F., Mustafa M. R., *et al.* (2011). *Journal of Medicinal Plants Research.* 5(23), 5534–5539. (b) Rotbart, H. A. (2000). *Antivir. Chem. Chemother.* 11, 261–271.
- [9] (a) Singh, A., & Rana, A. C. (2010). *J. Chem. Pharm. Res.* 2(1), 505–511. (b) Kaushik, S., Kumar, N., Drabu, S. (2010). *Pharma Res.* 3, 257–262.
- [10] Satyanarayana, M., Tiwari, Priti., Tripathi Brajendra, K., Srivastava, A. K., & Pratap, Ram. (2004). *Bioorg. Med. Chem.* 12(5), 883–889.
- [11] (a) Jung, Kyoung-H., Hyun, Soon-Y., Song, Dong-M., & Shin, Dong-Myung. (2002). *Opt. Mat.* 663–666. (b) Dong, Hoon-C., Young, Kwan-C. (2002). *Polymer.* 43, 703–710. (c) Keerti, M. N.,

- Sharanappa, T. N. (2013). *J. Luminescence*. 143, 484–491. (d) Afef, G., Michal, D., Vaclav, P., Taïcir, BenA. , & Rached, BenH. (2014). *J. Phys. Chem. Solids*. 75, 188–193. (e) Rajesh Kumar, P. C., Ravindracharya, V., Janardhanaa, K., Manjunathc, H. R., Karegouda, P., *et al.* (2011). *J. Mol. Struct.* 1005, 1–7.
- [12] (a) Xue, Y., Moua, Jie., Liua, Yi., Gong, X., Yang, Y., *et al.* (2010). *Cent. Eur. J. Chem.* 8(4) 928–936. (b) Tanaka, A., Nakashima, K., Miura Y. (2011). *Tetrahedron*, 67, 2260–2268.
- [13] (a) Patel, U. H., Gandhi, S. A., Barot, V. M., Patel, M. C. (2013). *Crystal Struct. Theory Appl.* 2, 167–175. (b) Patel, U. H., Gandhi, S. A., Barot, V. M. , & Patel, M. C. (2012). *Acta Cryst. E*68, o2926–o2927. (c) Patel, U. H., Gandhi, S. A. (2011). *Indian J Pure Appl. Phys.* 49, 263–269.
- [14] Sheldrick, G. M. *SHELX-97: Programs for the Solution and Refinement of Crystal Structures*, University of Gottingen: Gottingen, Germany, 1997.
- [15] Spek, A. L. (2009). *Acta Cryst. D*65, 148–155.
- [16] National Committee for Clinical Laboratory Standards (NCCLS). Reference method for broth dilution antifungal susceptibility testing of yeasts; approved standard-second edition, NCCLS document M27-A2. NCCLS, 940, West Valley Road. Suite (1400). Wayne, Pennsylvania, 19087–1898, USA. 2002 (. ISBN 1-56238-469-4).
- [17] Bernstein, J., Davis, R. E. , & Shimoni, L. (1995). *Angewandte Chemie*. 34(15),1555–1573.
- [18] Becke, A. D. (1993). *J. Chem. Phys.* 98, 1372–1377.
- [19] Jhonson, B. G., Gill, P. M. , & Pople, J. A. (1993). *J. Chem. Phys.* 98, 5612–5626. (b) Lee, C., Yang W., & Parr, R. G. (1988). *Phys. Rev. B* B37, 785–789.
- [20] Frisch, M. J., Trucks, G. W., Schlegel, H. B., Scuseria, G. E., Robb, M. A., *et al.* (2009). Gaussian 09, Revision D.01, Gaussian, Inc., Wallingford CT.
- [21] Dennington, R., Keith, T., & Millam, J. Semichem Inc., GaussView, Version 5, Shawnee Mission KS, 2009.
- [22] Betül Y., Hanife S., Nezihe Ç., Ibrahim Y., Alaaddin C. (2012). *J. Chem. Crystallogr.* 42, 897–904.
- [23] Namık, Ö., Eren, B., Dinçer, M., & Bekdemir, Y. (2010). *Mol. Phys.* 108(1), 13–24.